Comparative study of metallic silicide–germanide orthorhombic MnP systems

Damien Connétable[1] **and Olivier Thomas**[2]

[1] CIRIMAT, CNRS-INP-UPS UMR 5085, École Nationale d'Ingénieurs en Arts Chimiques et Technologiques (ENSIACET) 4, allée Émile Monso, BP 44362, F-31030 Toulouse Cedex 4, France
[2] Aix-Marseille Université, CNRS, IM2NP, UMR 7334, Campus de St Jérome, F-13397 Marseille Cedex, France

E-mail: damien.connetable@ensiacet.fr

Abstract
We present a comparative study of the structural, energetic, electronic and elastic properties of MX type MnP systems (where X = Si or Ge, and M = Pt, Pd or Ni) using first-principles calculations. The optimized ground state properties of these systems are in excellent agreement with the experimental values. A detailed comparative study of the elastic properties of polycrystalline structures is also presented. We analyze the relationship between the composition and the properties of the systems. Finally, we present the properties of $NiSi_{1-x}Ge_x$ alloys. We show that these properties depend linearly on the Ge content of the alloy. This work has important consequences for semiconductor devices in which silicides, germanides and alloys thereof are used as contact materials.

1. Introduction

Transition metal silicides are important contact materials for advanced field effect microelectronic devices. These materials are significant because of their metallic character and compatibility with silicon. More recently, SiGe alloys have been used to increase the mobility of charge carriers [1] or as sources of stresses in silicon channels, which also increase the mobility of the charge carriers [2]. Germanium or silicon–germanium alloys are contacted by forming transition metal germanides or silico-germanides. Most transition metals form isotopic silicides and germanides as full or extended solid solutions. In this study we focus on MX silicides or germanides (where M = transition metal and X = Si or Ge) that crystallize into orthorhombic MnP type structures. This behavior is especially observed for NiSi and NiGe, which are intermetallics that are currently used for contacting advanced electronic devices.

The NiSi structure has been studied at ambient pressure [3] and high pressures [4]; however, the effects of varying the composition (of the metal and/or the Si atoms) have not been investigated. The purpose of this study is to investigate the elastic properties of the MX-MnP systems and how the metal and/or Si/Ge affects these properties.

In section 2, we present the computational details for this study. The ground state properties (i.e., the lattice parameters, the formation energies and the electronic properties) of each alloy are presented and compared to each other in sections 3 and 4. In section 5, the elastic properties (mono- and polycrystalline) of all of the MX phases are presented. The anisotropies of these phases are then presented and compared with each other. We conclude in section 6 with a discussion on the energetic and elastic properties of $NiSi_{1-x}Ge_x$ alloys.

2. Computational details

The ground states of MX-MnP and the reference states (fcc and diamond phases) have been optimized by implementing DFT VASP [5]. Projected augmented wave pseudopotentials [6] were used. The spin-polarized version of the Perdew–Burke–Ernzerhof [7] (PBE) generalized gradient approximation (GGA) was used for the exchange–correlation functional. The structures were optimized by sampling the Brillouin zones using Γ-centered 25 × 25 × 25 and

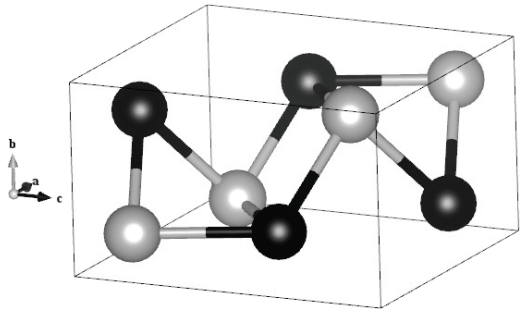

Figure 1. Schematic of the MnP structure: the metal atoms are shown in gray and the Ge/Si atoms are shown in black.

Table 1. Ground state properties of the reference states: lattice parameters (a_o, in Å), cohesive energies ($E_{\rm coh}$, in eV/atom), magnetic moments ($\mu_{\rm B}$, measured in Bohr units) and bulk modulus (B_o, in GPa); experimental data (from Kittel [9]) are provided for comparison.

			a_o	$E_{\rm coh}$	$\mu_{\rm B}$	B_o
Ni	fcc	Theo.	3.52	4.76	0.62	198
		Exp.	3.52	4.44	0.62	186
Pd	fcc	Theo.	3.96	3.71	0.33	163
		Exp.	3.89	3.89	0.0	181
Pt	fcc	Theo.	3.97	5.45	0.0	251
		Exp.	3.92	5.84	0.0	278
Si	diam	Theo.	5.47	4.56	0.0	90
		Exp.	5.43	4.63	0.0	99
Ge	diam	Theo.	5.77	3.74	0.0	57
		Exp.	5.68	3.85	0.0	77

15 × 25 × 15 Monkhorst and Pack grids [8] for the fcc and diamond systems and the MnP structures, respectively. Cut-off energies of 600 eV were used. We adopted the finest tetrahedron of 20 × 30 × 20 grids to calculate the electronic density of states (eDOS) and the formation energies for MnP systems.

The pseudo-potentials were tested on the reference phases. Table 1 shows that the lattice parameters, the cohesive energies, the magnetism and the bulk modulus are in good agreement with the experimental and theoretical literature. Two cases should be noted: Ge and Pd. We obtain a 'large' lattice parameter for germanium, which results in a softer bulk modulus than the experimental result. Our results for fcc-Pd are in agreement with previous theoretical work [10] on magnetism. We assumed that magnetic properties of the Pd alloys were not related to the results for fcc-Pd. All of the alloys were found to be non-magnetic.

3. Structural properties

The MX intermetallics, where M = Ni, Pt or Pd, and X = Si or Ge, crystallize in the MnP orthorhombic structure (space group 62, *Pnma*-D_{2h}^{16}, B31). The primitive cell is composed of eight atoms (oP8), where both atoms (M and X) are located in 4c Wyckoff positions (u_x, 1/4, u_z). Figure 1 is a schematic of the MnP structure.

Table 2 provides the optimized atomic positions which are weakly dependent on the compositions (of M and X).

Table 2. Wyckoff data for MnP systems, showing atoms in the 4c position (u_x, 1/4, u_z).

			u_x	u_z
NiSi	[3]	Ni	0.0085	0.1889
		Si	0.1795	0.5843
PdSi		Pd	0.0039	0.1912
		Si	0.1771	0.5732
PtSi		Pt	0.9964	0.1941
		Si	0.1791	0.5825
NiGe		Ni	0.0058	0.1908
		Ge	0.1905	0.5855
PdGe		Pd	0.0040	0.1907
		Ge	0.1859	0.5766
PtGe		Pt	0.9996	0.1925
		Ge	0.1859	0.5865

Table 3. Lattice parameters (in Å) and formation energies (in meV/atom) for MnP systems compared to experimental data.

	a_o	b_o	c_o	$E_{\rm f}$
NiSi	5.179[a]	3.365[a]	5.613[a]	−496[a]
	5.15[b]	3.35[b]	5.60[b]	
PdSi	5.638	3.469	6.177	−537
	5.65[b]	3.40[b]	6.15[b]	
PtSi	5.663	3.629	5.998	−671
	5.600[c]	3.584[c]	5.924[c]	−670[c]
	5.61[b]	3.60[b]	5.95[b]	−620[d]
NiGe	5.419	3.464	5.864	−313
	5.40[b]	3.45[b]	5.85[b]	
PdGe	5.970	3.565	6.367	−458
	5.80[b]	3.50[b]	6.36[b]	
PtGe	5.842	3.743	6.187	−475
	5.75[b]	3.72[b]	6.11[b]	

[a] Theo. PBE [3]. [b] Exp. [11]. [c] Theo. LDA [12]. [d] Exp. [13].

Table 3 shows that the optimized lattice parameters, in contrast, depend strongly on the species. The lattice parameters are in excellent agreement with the low temperature experimental data [11]. In all of the cases, the GGA simulations produce slightly higher lattice parameters than the experimental results, unlike the results obtained using LDA functionals. For PtSi, Beckstein *et al* [12] found lattice parameters smaller than those reported here or those obtained from experimental measurements. These differences lead to significant changes in the PtSi properties and the elastic properties in particular (see below).

Comparing the results for all of the systems shows that the lattice parameters of each phase are highly dependent on the phase composition. Steric effects may be used to explain the primary changes in the lattice parameters of the MGe/Si systems. We illustrate this result by evaluating the relative decrease in the lattice parameters between Si and Ge (a(Si)/a(Ge)) for each of the three metals. For all of the systems, we find a ratio of approximately 0.97 between Si and Ge, which is equivalent to the one found for the Si/Ge diamond structure.

We also find that all of the phases are highly stable with respect to their reference states: the stability increases with

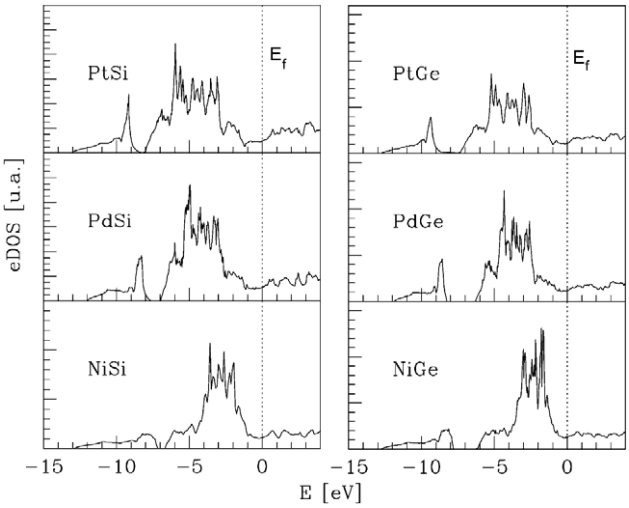

Figure 2. Electronic density of states of MX-MnP; the NiSi values are plotted from the results in [3].

Table 4. Density of states at the Fermi level ($N(E_f)$, in states eV^{-1}) for different elements.

X\M	Ni	Pd	Pt
Si	2.20	2.16	1.99
Ge	2.44	2.24	2.19

the weight of the metal atom. All of the structures are metallic (see the electronic properties given above) and non-magnetic.

4. Electronic properties

Figure 2 shows the electronic density of states (eDOS). Note that all of the eDOSs are extremely similar, especially for the same metal, suggesting that the metal controls the electronic properties.

We analyze each system more precisely by projecting the density of states (pDOS) onto the orbitals (not shown here). The pDOSs are extremely similar to those reported for NiSi in [3]. At low energies, we find the M and X s shells; near the Fermi level, the p shells of X and d orbitals of the metals are hybridized. The p and s shells of the Ge systems are slightly more contracted, thereby inducing a larger gap in the valence bands. At the Fermi level, the density of states is always localized near a minimum. Table 4 shows the density of states at the Fermi level ($N(E_f)$) for reference. For all of the systems, $N(E_f)$ is approximately 2 states eV^{-1} and is approximately 10% larger for Ge systems than for Si systems.

5. Elastic properties

The elastic constants were calculated using the same methodology as the one presented in [3]. The elastic properties of orthorhombic systems are characterized by nine elastic constants, corresponding to the six diagonal terms (C_{ii}, where $i = 1, \ldots, 6$) and three off-diagonal terms (C_{12}, C_{13} and C_{23}). The elastic constants and the bulk modulus are listed in table 5.

The elastic constants of the Pd alloys are smoother (by 10–15%) than those for Ni and Pt systems (as for the reference states). The elastic constants for the Ge alloys are also approximately 20% smoother than those for Si systems. This evolution can be related to the decrease in the lattice parameters across the systems.

Our results for PtSi are clearly different from those reported by Beckstein [12], i.e., our results are 10% smaller than Beckstein's results. This difference can be attributed to two main effects: the differences between the lattice parameters and overestimates of the binding energy, i.e., bonds are stronger within the LDA.

We deduce the mono- and polycrystalline elastic properties of the system from these data and analyze the anisotropies. Following [3], we compute the elastic properties of the polycrystalline structures: the shear and bulk moduli (G and B) using the Voigt, Reuss and Hill approximations, Young's modulus (Y), Poisson's ratio (ν), and the bulk modulus along different axes. The results are summarized in table 6.

Note that the 'average' mechanical properties, i.e., ν, G and B, depend weakly on the alloy composition. In contrast, and as reported in our results for the lattice parameters, the bulk modulus along the crystallographic axes and the Young's modulus are strongly anisotropic. This anisotropy is illustrated in figure 3. The anisotropic values are given in table 7. The anisotropy decreases when going from Ni to Pt (see table 8). Germanides are softer than silicides, which is consistent with the lower melting points of germanides relative to silicides. However, germanides exhibit a slightly more pronounced anisotropy than silicides. The Young's modulus is smallest along the [010] direction and largest along the [111] direction (see table 7): the anisotropy ratio ranges

Table 5. Elastic constants (C_{ij}) and bulk modulus (B) (in GPa) of MnP systems.

		C_{11}	C_{22}	C_{33}	C_{44}	C_{55}	C_{66}	C_{12}	C_{13}	C_{23}	B_v
NiSi	[3]	272	222	229	106	128	126	166	94	149	171
PdSi		228	167	230	77	90	75	126	104	142	152
PtSi		259	240	274	88	89	50	136	101	136	169
	[12]	298	269	308	100	104	66	156	132	165	198
NiGe		193	167	172	71	102	104	136	92	116	136
PdGe		179	139	175	60	74	69	112	87	110	124
PtGe		202	192	199	68	73	53	124	102	112	141

Table 6. Isotropic values of the shear and bulk moduli (in GPa) using the Voigt, Reuss and Hill approximations (which are labeled as V, R, and H, respectively); Young's modulus (in GPa), the Poisson's ratio (ν) and the bulk modulus (in GPa) along the crystallographic axes a, b and c (see [14], appendix) are also provided.

		G_R	G_V	G_H	B_R	B_V	B_H	E	ν	B_a	B_b	B_c
NiSi	[3]	65	93	79	168	171	170	205	0.30	486	957	352
PdSi		50	65	57	150	152	151	153	0.33	532	298	702
PtSi		67	72	69	169	169	169	183	0.32	469	537	517
	[12]	77	82	80	198	198	198	211	0.32	572	575	639
NiGe		68	68	56	134	136	135	147	0.32	419	605	292
PdGe		39	53	46	123	124	124	122	0.33	455	283	418
PtGe		56	56	54	141	141	141	144	0.33	445	449	381

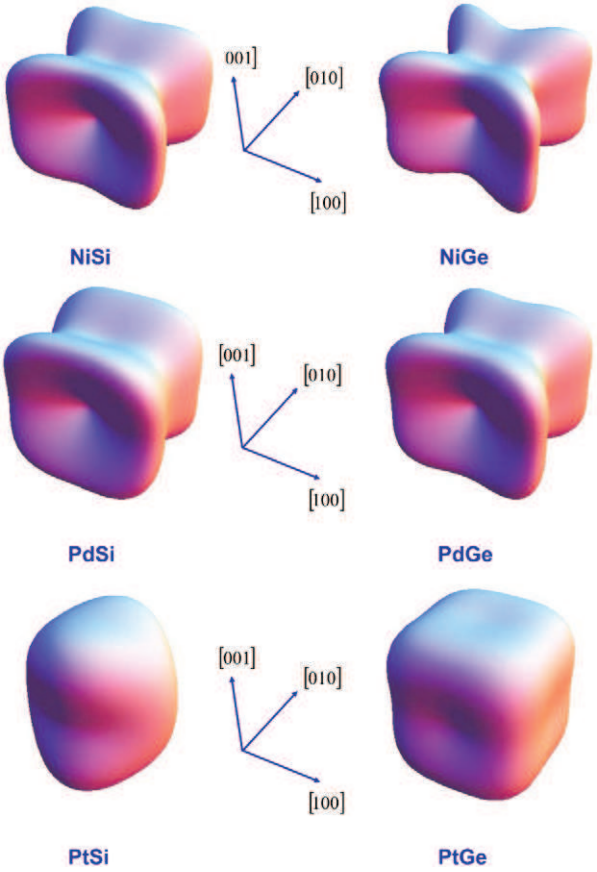

Figure 3. 3D representations of the Young's modulus.

Table 7. Young's modulus (in GPa) along different crystallographic directions.

		E_{100}	E_{010}	E_{001}	E_{111}	E_{111}/E_{010}
NiSi	[3]	146	78	127	235	3.0
PdSi		133	58	109	183	3.1
PtSi		179	140	194	193	1.4
	[12]	201	150	200	226	1.5
NiGe		83	51	91	177	3.5
PdGe		88	45	88	146	3.2
PtGe		115	100	127	164	1.6

Table 8. The anisotropy in the shear elastic factor (A_i, where $i = 1, 2, 3$), the anisotropy in the directional bulk modulus (A_{B_a}, A_{B_c}) and the anisotropy in the compressibility and the shear modulus (A_B and A_G in %).

		A_1	A_2	A_3	A_{B_a}	A_{B_c}	A_B	A_G
NiSi	[3]	1.35	3.37	3.13	0.51	0.37	1.0	17.7
PdSi		1.23	3.19	2.10	1.78	2.36	0.6	13.6
PtSi		1.06	1.47	0.87	0.87	0.96	0.04	3.6
NiGe		1.55	3.84	4.67	0.69	0.48	0.7	22.5
PdGe		1.34	3.18	2.96	1.60	1.47	0.2	15.5
PtGe		1.39	1.75	1.44	0.99	0.85	0.06	3.3

from 1.5 to 3.5, depending on the composition. Analysis on the anisotropy in the shear factors (see table 8) results in the same conclusion.

All of these results suggest that the anisotropy is controlled mainly by the nature of the metal.

We conclude our analysis of the anisotropy in MnP systems with a discussion of the Poisson's ratio, ν. In cubic systems, ν lies within the range $[-1, \frac{1}{2}]$. However, many studies have shown (see for example [15]) that the Poisson's ratio in non-cubic systems is not bounded from either above or below. In the appendix, we present the equations for computing the Poisson's ratio in a direction ($\mathbf{m}$) perpendicular to a different stress direction ($\mathbf{n}$). In table 9, we report $\nu^{\mathbf{m}}_{\mathbf{n}}$, where $\mathbf{m}$ and $\mathbf{n}$ are along the main directions (x, y and z). The elastic behavior observed under a uniaxial strain is clearly different from the elastic behavior of cubic systems. In some cases, the value of ν is larger than 0.5 (as in $\nu^{0,1,0}_{1,0,0}$, for example). Moreover, when the system is stressed along $\mathbf{n} = a$ (or c), a strong contraction ($\nu^{0,1,0}_{1,0,0} > 0.5$) is observed along the b direction, whereas the system expands slightly ($\nu^{0,0,1}_{1,0,0} < 0$) along the c axis for NiSi, PdSi, NiGe and PdGe. These results may be correlated with the thermal expansion of the lattice parameters: the b axis contracts and the a and c axes expand over the temperature range between 293 and 700 K [11, 16] for these systems; however, a clear explanation is not yet available.

6. Effect of the composition on the elastic properties in $NiSi_{1-x}Ge_x$

In this section, the effect of the composition on the elastic properties of $NiSi_{1-x}Ge_x$ alloys is presented. Variations in the Ge content in NiX systems and intermediate compositions

Table 9. Anisotropy in the Poisson's ratio, $\nu_{\mathbf{n}}^{\mathbf{m}}$, for **m** and **n** along the $\{x, y, z\}$ axes.

	$\nu_{1,0,0}^{0,1,0}$	$\nu_{1,0,0}^{0,0,1}$	$\nu_{0,1,0}^{1,0,0}$	$\nu_{0,1,0}^{0,0,1}$	$\nu_{0,0,1}^{1,0,0}$	$\nu_{0,0,1}^{0,1,0}$
NiSi	0.84	−0.14	0.45	0.47	−0.12	0.76
PdSi	0.78	−0.03	0.34	0.46	−0.02	0.87
PtSi	0.50	0.12	0.39	0.35	0.13	0.49
NiGe	0.83	−0.03	0.51	0.41	−0.04	0.72
PdGe	0.83	−0.02	0.42	0.42	−0.02	0.81
PtGe	0.51	0.23	0.45	0.33	0.25	0.42

Table 10. Lattice parameters (in Å), volume (V_o, in Å^3), and formation energies (E_f, in meV/atom) of $NiSi_{1-x}Ge_x$ systems, for various values of the Ge content x.

x	E_f	a_o	b_o	c_o	V_o
0	−503	5.165	3.378	5.621	98
0.25	−446	5.247	3.376	5.700	101
0.50	−400	5.346	3.393	5.742	104
0.75	−353	5.358	3.435	5.806	107
1	−313	5.419	3.464	5.864	110

were studied further by sequentially replacing a Si atom by a Ge atom.

Ground state properties. Calculations were performed on a primitive cell (eight atoms), and all of the configurations (at each Ge content) were used to evaluate the effect of the composition on the ground state properties. Equivalent results were obtained for each configuration studied at a given Ge content (the difference in energies and lattice parameters is negligible); therefore we only list the results (the lattice parameters and the formation energies) for one configuration in table 10. Substituting Si with Ge induces a monotonic change in the energy. To illustrate this result, we use a linear regression to fit the formation energy as a function of the Ge content (x, in %). We obtain the following expression (with a correlation factor of $R^2 = 1$):

$$E_f(x) = -497 + 189x. \quad (1)$$

An equivalent relation can be found for the evolution of the volume. We find that the volume of the cell increases linearly with the Ge content: $\sim 98 + 12x$ (in Å^3).

To confirm these results, we investigate the ground state properties for larger supercells. Intermediate Ge(Si) contents, i.e., $Ni_{32}Si_xGe_{32-x}$, are simulated using $2 \times 2 \times 2$ supercells. For x ranging from 0 to 32, we consider only one configuration (the inter-atomic forces and the stresses on boxes are also

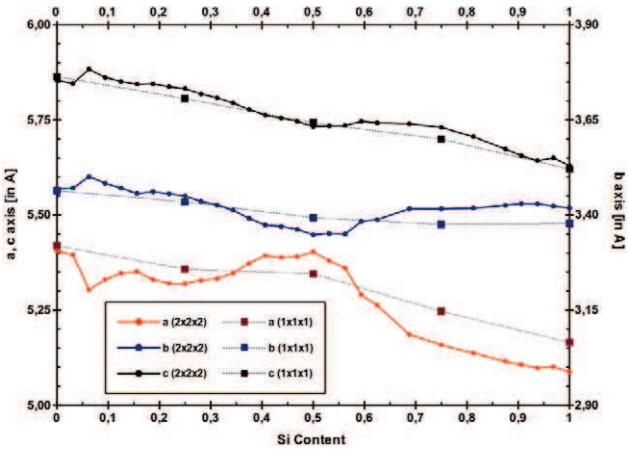

Figure 4. Evolution of the lattice parameters in $NiSi_xGe_{1-x}$ systems as a function of x; the dashed lines represent data computed using a primitive cell, and the lines represent data for the lattice parameters computed using $2 \times 2 \times 2$ supercells.

fully relaxed). The orthorhombic symmetries of the supercells are almost completely preserved in the final structures, which exhibit a low crystalline anisotropy (i.e., less than 10^{-4}) even at intermediate Ge(Si) contents. The evolutions of the formation energies and the volumes with the Ge content are found to be equivalent using the primitive cell and the supercell. Figure 4 shows that the lattice parameters do not evolve monotonically, despite the overall increase in the lattice parameters for the systems containing Si. These results confirm that the evolution of the lattice parameters is mainly controlled by steric effects.

Evolution of elasticity for systems containing Ge. Our results for the ground state properties suggest that the elastic properties of these systems should change monotonically with the Ge content. We computed the elastic constants for three intermediate Ge contents using the primitive cell (corresponding to one configuration for each content value). Table 11 shows the results of these simulations (C_{ij}). Figure 5 shows the evolution of these elastic constants. The elastic constants clearly evolve linearly with x. Within a first-order approximation, the properties of MSiGe alloy (where M = Pt or Pd) structures can be interpolated linearly from extreme systems (NiSi and NiGe).

7. Conclusion

In this study, we have presented first-principles calculations of the ground states (X = Si or Ge, and M = Ni, Pd or

Table 11. Evolution of the elastic constants (in GPa) with the Ge content in $NiGe_xSi_{1-x}$.

x	C_{11}	C_{22}	C_{33}	C_{44}	C_{55}	C_{66}	C_{12}	C_{13}	C_{23}	B_v
0	272	222	229	106	128	126	147	94	149	171
0.25	248	202	218	95	123	120	153	85	138	158
0.50	222	186	201	88	114	113	149	97	134	152
0.75	208	179	188	79	109	111	144	98	127	146
1	193	167	172	71	102	104	136	92	116	136

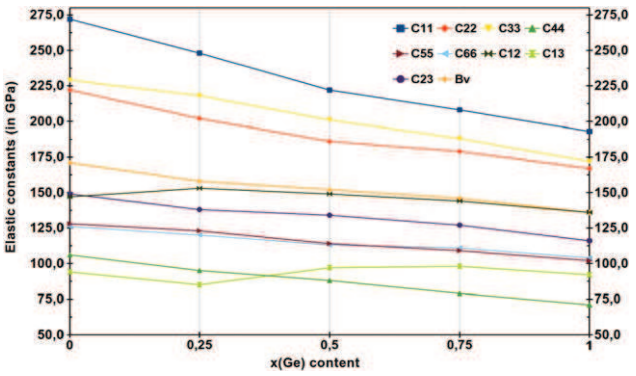

Figure 5. Evolution of the elastic constants with the Ge content.

Pt) of MX-MnP structures. The structural, electronic and elastic properties of ideal structures were calculated using density functional theory. We showed that the main structural differences between Si and Ge systems can be attributed to steric effects. These systems exhibit a strong elastic anisotropy, which fades upon changing the metal species from Ni to Pt.

To illustrate these steric effects, we performed simulations on $NiSi_{1-x}Ge_x$ alloys. We showed that the properties of these alloys can be satisfactorily linearly interpolated based on the Ge content. We propose that these results can be extrapolated to Pt and Pd alloys.

Acknowledgments

This work was granted access to the HPC resources of CALMIP (CICT Toulouse, France) under the allocation 2012-p0912.

Appendix. Anisotropy in Poisson's ratio

In general, Poisson's ratio (ν) in non-cubic systems is considered to be an 'average' value, which is computed as follows:

$$\nu = \frac{3B - 2G}{2(3B + G)}. \tag{2}$$

However, ν depends on the transverse contraction under the application of a uniaxial stress. Boulanger *et al* [17] have shown that Poisson's ratio ($\nu = \nu_{\mathbf{n}}^{\mathbf{m}}$) depends on the direction **n** of the applied tension and **m**, which is orthogonal to **n**. We can calculate Poisson's ratio for the application of a stress along the x, y or z axis in orthorhombic systems as follows:

$$\nu_{1,0,0}^{0,\cos\theta,\sin\theta} = \frac{C_{12}C_{33} - C_{13}C_{23}}{C_{22}C_{33} - C_{23}^2}\cos^2\theta + \frac{C_{13}C_{22} - C_{12}C_{23}}{C_{33}C_{22} - C_{23}^2}\sin^2\theta \tag{3}$$

$$\nu_{0,1,0}^{\sin\theta,0,\cos\theta} = \frac{C_{23}C_{11} - C_{12}C_{13}}{C_{33}C_{11} - C_{13}^2}\cos^2\theta + \frac{C_{12}C_{33} - C_{23}C_{13}}{C_{11}C_{33} - C_{13}^2}\sin^2\theta \tag{4}$$

$$\nu_{0,0,1}^{\cos\theta,\sin\theta,0} = \frac{C_{13}C_{22} - C_{12}C_{23}}{C_{11}C_{22} - C_{12}^2}\cos^2\theta + \frac{C_{23}C_{11} - C_{12}C_{13}}{C_{11}C_{22} - C_{12}^2}\sin^2\theta \tag{5}$$

where θ represents the direction of **m** in the plane perpendicular to **n**, i.e., $\mathbf{m} = (0, \cos\theta, \sin\theta)$.

References

[1] Thompson S E *et al* 2004 *IEEE Electron Device Lett.* **25** 191
[2] Patton G L, Iyer S S, Delage S L, Tiwari S and Stork J M C 1988 *IEEE Electron Device Lett.* **9** 165
[3] Connétable D and Thomas O 2009 *Phys. Rev.* B **79** 094101
[4] Vocadlo L, Wood I G and Dobson D P 2012 *J. Appl. Crystallogr.* **45** 186–96
[5] Kresse G and Hafner J 1993 *Phys. Rev.* B **47** 558
Kresse G and Hafner J 1994 *Phys. Rev.* B **49** 14251
Kresse G and Furthmüller J 1996 *Phys. Rev.* B **54** 11169
Kresse G and Furthmüller J 1996 *Comput. Mater. Sci.* **6** 15
[6] Kresse G and Joubert D 1999 *Phys. Rev.* B **59** 1758
[7] Perdew J P, Burke K and Ernzerhof M 1996 *Phys. Rev. Lett.* **77** 3865
Perdew J P, Burke K and Ernzerhof M 1997 *Phys. Rev. Lett.* **78** 1396
[8] Monkhorst H J and Pack J D 1976 *Phys. Rev.* B **13** 5188
[9] Kittel C 1996 *Introduction to Solid State Physics* (New York: Wiley)
[10] Chepulskii R V, Barabash S V and Zunger A 2012 *Phys. Rev.* B **85** 144201
[11] Brondeel L and Detavernier C 2009 *Report on 'In situ' XRD thermische expansie van materialen*
[12] Beckstein O, Klepeis J E, Hart G L W and Pankratov O 2001 *Phys. Rev.* B **63** 134112
[13] Chandrasekharaiah M S, Margrave J L and O'Hare P A G 1993 *J. Phys. Chem. Ref. Data* **22** 1459
[14] Ravindran P, Fast L, Korzhavyi P A, Johansson B, Wills J and Eriksson O 1998 *J. Appl. Phys.* **84** 4891
[15] Ting T C T and Chen T Y 2005 *Q. J. Mech. Appl. Math.* **58** 73–82
[16] Wilson D F and Cavin O B 1992 *Scr. Metall. Mater.* **26** 8
[17] Boulanger P H and Hayes M 1998 *J. Elasticity* **50** 87–9